ACS OMEGA

Open Access



http://pubs.acs.org/journal/acsodf

Article

# Charge Effects and Electron Phonon Coupling in Potassium-Doped Graphene

Dario Marchiani,* Riccardo Frisenda, Carlo Mariani, Marco Sbroscia, Tommaso Caruso, Oreste De Luca, Marco Papagno, Daniela Pacilé, Samuel Jeong, Yoshikazu Ito, and Maria Grazia Betti*

Cite This: *ACS Omega* 2024, 9, 39546−39553

Read Online

ACCESS | Metrics & More | Article Recommendations | Supporting Information

**ABSTRACT:** Herewith, we propose a comprehensive study of the vibrational response of chemical doping of free-standing graphene (Gr). Complementary insights on the increased metallicity have been demonstrated by the emerging plasmon excitation in the upper Dirac cone, observed by inelastic electron scattering and core-level photoemission. The electron migration in the $\pi^*$ upper Dirac band unveils an electron−phonon coupling of contaminant-free K-doped Gr, as evidenced by advanced micro-Raman spectroscopy in ultrahigh vacuum ambient. The vibrational response of potassium-doped Gr correlated with the charge injected in the upper Dirac cone, and the Fermi level shift unravel a notable electron−phonon coupling, which is stronger than that observed for gate voltage-doped Gr.

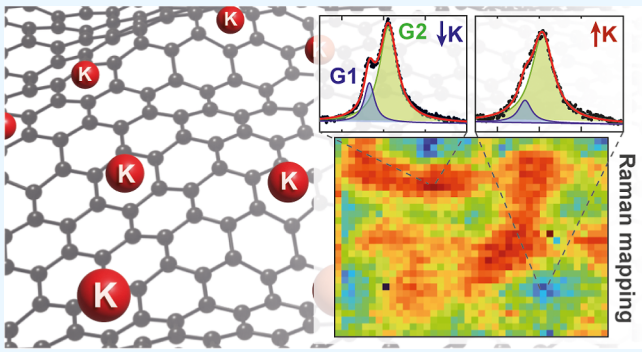


## INTRODUCTION

Enhanced metallicity and higher density of electronic states at the Fermi level in graphene (Gr)[1,2] can be tuned by varying the charge density by electric or chemical doping. The electron migration in the upper Dirac cone influences the electron−phonon interaction, as extensively demonstrated in theoretical predictions and in pioneering Raman experiments on Gr mode evolution as a function of doping.[1,2]

It is worth noting that most of the Raman investigations were performed in the low doping regime by electric field effect,[1,3−5] while an efficient method to achieve high n-type chemical doping can be alkali metal (AM) adsorption on Gr.[6] Though electric doping by gate voltages gives the advantage of inducing a homogeneous shift of the Fermi level over all the sample, the chemical doping allows one to control the Fermi level position in a wide energy range with an enhanced electron−phonon interaction, as observed for potassium-doped graphite.[7] Furthermore, experimental evidence of increased electron−phonon interaction and quantification of the relevant $\lambda$ parameter in AM-doped Gr has been deduced by angular-resolved photoelectron spectroscopy (ARPES),[7−10] while Raman has been used mainly for low electric field-effect doping.[3,11−13] However, it has been clearly remarked that ARPES gives an overestimation of $\lambda$ for AM-doped Gr.[14] Thus, a thorough Raman study on highly controlled AM-doping of Gr in different forms (fully free-standing or supported flakes) is still lacking.

In order to deduce the electron−phonon interaction coupling from a Raman study of AM-doped Gr, critical issues are the in situ deposition of AMs in ultrahigh vacuum (UHV) ambient and the choice of suitable high-quality free-standing Gr samples. In fact, previous experimental studies on chemically doped Gr were mostly performed by exposing single-layer or few-layer Gr samples to AMs in a controlled atmosphere,[6,15] except a single example—to our knowledge—of Raman spectroscopy for Cs-doped Gr/Ir(111) carried out in UHV.[16] Furthermore, a fine control of the evolution of the electronic response at increasing degree of metallicity of Gr obtained by AM doping has been rarely employed in free-standing Gr, without detrimental effects of an underlying substrate. On the other side, Gr flakes have been electron doped mainly via electric field-effect doping[1,3,4] and without discriminating its dependence on the number of Gr layers involved in the process.

In this paper, we overcome these crucial challenges, investigating by UHV micro-Raman spectroscopy of highly controlled potassium-doped fully free-standing nanoporous Gr (NPG), a defect-free single- or bi-Gr (2L) layer(s) with high specific surface area.[17−20] AMs can adsorb on NPG strongly enough on the surface to form a thermodynamically stable arrangement. A comprehensive view of the vibrational

Received: April 12, 2024
Revised: April 24, 2024
Accepted: April 26, 2024
Published: September 9, 2024

response and electron−phonon coupling (EPC) of contaminant-free K-doped Gr has been unveiled thanks to a new original advanced experimental setup combining AM in situ deposition with micro-Raman and high-resolution X-ray photoelectron spectroscopy (XPS) in UHV ambient (see Supporting Information). A complementary electron energy loss spectroscopy (EELS) investigation correlates the occupation of the $\pi^*$ conduction band with the Dirac plasmon evolution. Furthermore, comparison with K-doped flat 2-layer Gr flakes allows one to determine the doping associated with the donated charge and that induced by strain effects in the Raman response as a function of K doping for these free-standing Gr prototypes.

These correlated experimental findings on the plasmonic response in chemically doped free-standing Gr are in excellent agreement with the vibrational frequency shift due to electron−phonon interaction driven by the K charge migration, as interpreted by UHV Raman spectroscopy. This allows a fine control of the evolution of the vibrational response to experimentally determine the strength of EPC, which is higher than in doped Gr by electric field effect.

## RESULTS AND DISCUSSION

AM doping of Gr, avoiding any substrate influence, can be successfully achieved by employing NPG, a fully free-standing sheet with large areas in closed tubular forms decorated by pores at the micrometer scale, as depicted in the scanning electron microscopy (SEM) image shown in Figure 1a. The transmission electron microscopy (TEM) image (inset) enlightens the crystalline order of the hexagonal mesh at the nanoscale. The hexagonal moiré superstructure visible in the TEM image suggests the presence of misoriented non-Bernal-stacked bilayers.[18] In fact, NPG is a bicontinuous interconnected arrangement of high-quality Gr veils, dominated by the presence of single or weakly interacting bilayer(s) of Gr, stacked in a twisted turbostratic arrangement, as assessed in recent studies.[17−21]

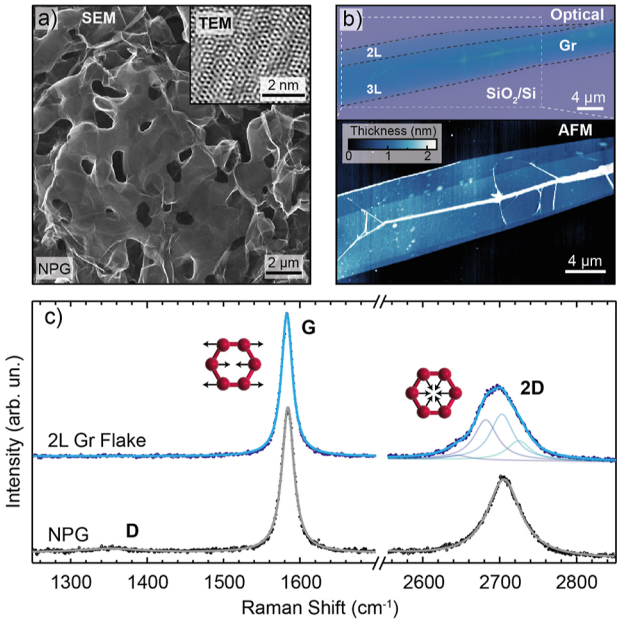


**Figure 1.** (a): SEM image of the NPG sample (14.5 × 14.5 $\mu m^2$) and the TEM image in the inset (5.5 × 4.5 $nm^2$). (b) Upper panel: optical image (42 × 18 $\mu m^2$) of the Gr flake on a $SiO_2$/Si substrate, with bilayer and trilayer regions; lower panel: AFM image in a region of the Gr flake zoomed from the upper panel. (c) Micro-Raman spectra in UHV for the 2L Gr flake (upper spectrum) and NPG (lower spectrum), taken with 532 nm laser wavelength; the dots are experimental points, and the solid lines represent the resulting fit (see main text description); the bilayer Gr presents the typical multicomponent 2D band mode, while the NPG is well-fitted with a single Lorentzian component due to the turbostratic layer stacking.

The three-dimensional (3D) architecture of the large size (∼1 × 1 $cm^2$) NPG sample is compared with the few-layer Gr flat flake deposited on a $SiO_2$/Si substrate, as reported in Figure 1b. The optical image of the exfoliated flake (top of Figure 1b) reveals two regions, a 2-layer (2L) and 3-layer (3L) zone, as estimated by optical transmission (see Experimental Methods below), compatible with the typical absorption coefficient of 2.3% per Gr layer.[22] A further proof of the Gr flake topography was obtained via atomic force microscopy (AFM), whose topographic image is displayed in the lower side of panel (b), where the step between the 2L and 3L Gr flake displayed through the color scale is ∼0.4 nm.

Raman spectroscopy has been by far the benchmark technique for determining the Gr quality and number of layers,[23,24] and it is apt to compare the hallmarks of NPG with a 2-layer Gr flake. Representative $\mu$-Raman spectra of the large-sized NPG sample and of a micron-sized region of the Gr flake with the resulting Raman band fits are shown in panel (c) of Figure 1. At first glance, both Raman spectra present similar peaks. The G band around 1580 $cm^{-1}$, with $E_{2g}$ symmetry, is related to a first-order process involving an iTO or iLO phonon mode at $q = 0$ momentum, associated with an in-plane out-of-phase displacement of the atoms. The D band (1350 $cm^{-1}$) related to a second-order process and activated only in the presence of defects, absent in the flat exfoliated Gr flake, is only slightly detectable in NPG due to the presence of bent regions of the sample. The 2D band, roughly centered at 2700 $cm^{-1}$ and associated with the breathing of the carbon atoms ring, is activated by a second-order process involving two iTO phonons with finite momentum $\boldsymbol{K}$ and requires a scattering from a K point to a K′ point of the Brillouin zone. The 2D band line shape for NPG differs from that of the 2L Gr flake (Figure 1c). In fact, the splitting of the band structure in the AB-stacked bilayer Gr flake causes four actual scattering processes in the electronic bands, reflected in a complex 2D Raman band line shape, fitted with the expected four components.[24] On the other hand, NPG mostly composed by 2L Gr veils of weakly interacting layers in mismatched angle turbostratic stacking[18] presents a 2D band line shape narrower than the 2L Gr flake.

Recently, it has been shown that potassium doping of NPG induces an enhanced metallicity.[25] In fact, the charge donated by the K adatoms to the $\pi^*$ Gr states, upshifts the Fermi level with respect to the Dirac cone, inducing plasmonic excitations associated with the collective longitudinal excitation of the electrons in the conduction band. This collective excitation can be directly probed via EELS. The evolution of the EELS spectra taken with a primary beam of $E_p$ = 105.5 eV in reflection geometry, for the K/NPG system at increasing K exposures, is shown in Figure 2a. The main loss feature of the clean NPG is the $\pi$ plasmon at 6.6 eV, whose energy position and asymmetric line shape are due to the blueshift of the energy dispersion,[26−29] hidden here by an average along the symmetry directions due to the warped 3D morphology of the NPG sample. Upon increasing potassium doping, a prominent


https://doi.org/10.1021/acsomega.4c03543
ACS Omega 2024, 9, 39546−39553

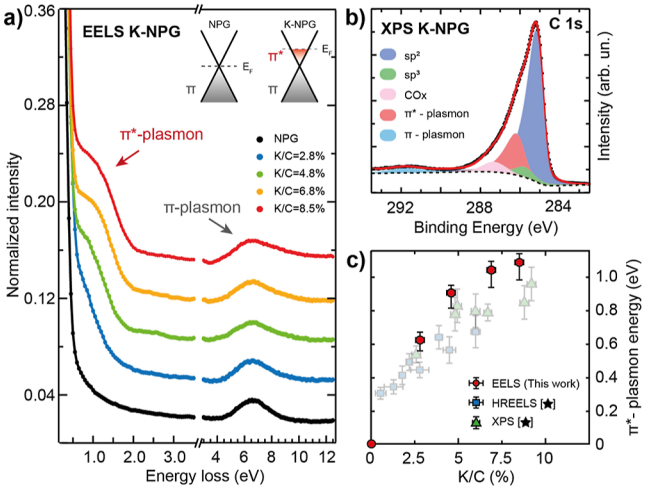


**Figure 2.** (a) EELS spectra of K-NPG as a function of K coverage, taken with $E_p$ = 105.5 eV, showing both the $\pi$ and $\pi^*$ plasmon excitations; inset: scheme of the rigid band model upon electron doping; (b) C 1s core level of K-NPG at a K/C = 8.5 at. % concentration, collected with monochromatized Al K$\alpha$ radiation (1486.6 eV) on the same sample surface of the EELS measurements: experimental data (black dots), fitting curve (red line), single fitting components as in the legend (colored curves); (c) $\pi^*$-plasmon energy as a function of K doping, deduced from the EELS experiment (red symbols), and comparison with the plasmon energy as derived from previous high-resolution-EELS and XPS data [★][25] (light gray symbols).

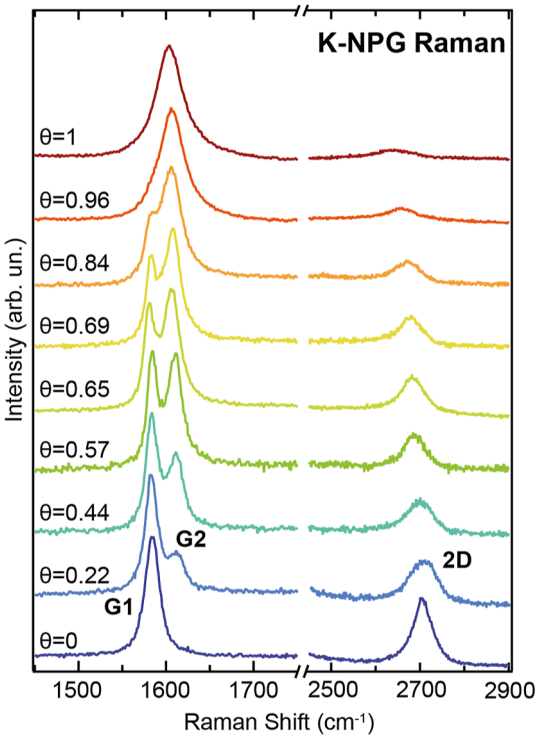


**Figure 3.** Selected Raman spectra of K-NPG as a function of K coverage ($\Theta$, defined as $\left(\Theta = \frac{I_{G2}}{I_{G1}+I_{G2}}\right)$) up to saturation coverage, in the G and 2D Raman band wavenumber range, taken with 532 nm laser wavelength.

shoulder, close to the elastic peak tail, emerges with increasing energy loss as a function of the doping level, up to 1.1 eV at saturation (panel c). This feature can be related to a plasmonic excitation due to the electrons in the $\pi^*$ upper Dirac cone, while the $\pi$ plasmon remains almost unperturbed, apart from a slight broadening at increasing K dose, probably associated with a slight momentum-averaged energy shift.

Evidence of the Dirac plasmon can also be obtained by the analysis of the line shape of the C 1s XPS spectra, as shown in Figure 2b for the K/C = 8.5% doping level, whose evolution is discussed in detail in ref 25. The peak asymmetry at high binding energy can be attributed to a metallic tail due to electron−hole pair transitions from the $\pi$ to $\pi^*$ band and to the presence of the extrinsic $\pi^*$ plasmon close to the main $sp^2$ component, excited by the outcoming photoelectrons.[25] The Dirac $\pi^*$-plasmon energy evolution as a function of K doping as measured by EELS is shown in Figure 2c, presenting a good agreement with previous high-resolution-EELS and XPS measurements.[25]

A cross-correlation of different experimental techniques can better enlighten how the electronic quasi-particle spectrum is related to the vibrational Raman response. It is also well established that Raman bands in doped Gr are influenced by the increased charge carrier density in the upper Dirac cone due to the modified electron−phonon interaction.[30−35] In Figure 3, the evolution of a selected data set of Raman spectra of NPG upon increasing potassium doping is presented.

At the first K doping, the pristine G band at 1584 $cm^{-1}$ (hereon named G1) decreases in intensity, while a new component (G2) appears at about 1611 $cm^{-1}$, and the 2D band starts reducing its intensity. Upon increasing the K dose, the weight intensity of the G2 band continuously increases relative to the G1, whereas the 2D band intensity decreases until quenching at full coverage $\left(\Theta = 1, \text{ where } \Theta = \frac{I_{G2}}{I_{G1}+I_{G2}}\right)$. The appearance of the G2 peak is a hallmark of the breakdown of the Born−Oppenheimer (BO) approximation, and its frequency shift with respect to G1 is due to a nonadiabatic contribution, as predicted by Pisana et al.[1] The coexistence of the G1 and G2 bands at low coverage is due to the potassium-uncovered regions of the NPG surface (the latter still showing the G1 peak). As more charge is donated to the system, the doping becomes more homogeneously distributed on the whole NPG surface, resulting in the reduction of the G1 band intensity, up to a complete disappearance when the saturation value is reached.

Most of the experimental studies on charge doping of Gr have been carried out by gate voltage application,[1,3,5,11,12,36] thus inducing a homogeneous overall shift of the electronic bands with respect to the Fermi level. By doping Gr with AMs, a more complex process is present since the charge donation takes place at and around the sites where the AM adsorbs, and it is dependent on the size of the AM-covered area. This accounts for the coexistence of the G1 and G2 bands before K-doping saturation of the NPG sample.

In order to probe the homogeneity of the K doping in NPG, a micro-Raman mapping of highly doped K-NPG has been done, over a region of 20 × 15 $\mu m^2$ in steps of 500 nm, leading to the best resolution possible (given the laser excitation wavelength of 532 nm), as reported in Figure 4. The color scale in both panels (a) and (b) suggest a very homogeneous distribution of potassium uptake, with only slight variation at the micrometer scale. In fact, the $\Theta = \frac{I_{G2}}{I_{G1}+I_{G2}}$ parameter spatial distribution shows a homogeneous doping level, quantified by


https://doi.org/10.1021/acsomega.4c03543
ACS Omega 2024, 9, 39546−39553

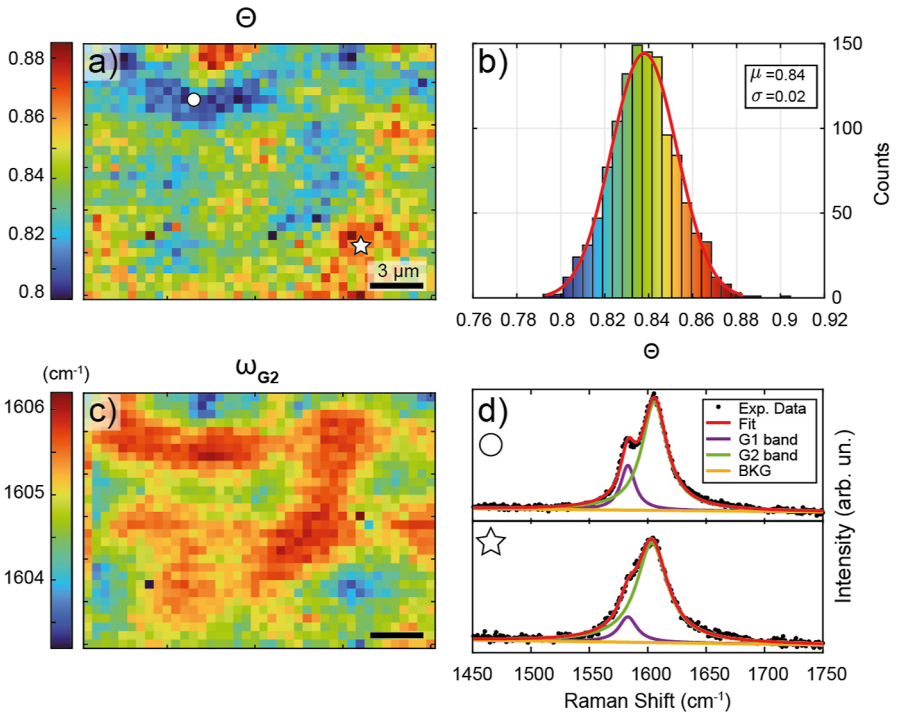


**Figure 4.** (a) Spatial Raman mapping of coverage $\Theta = \frac{I_{G2}}{I_{G1}+I_{G2}}$, taken at a highly doped K-NPG sample, in a 20 × 15 $\mu m^2$ spatial region, with 500 nm steps; the homogeneity in *K* coverage can be deduced from the histogram of the Θ value distribution reported in panel (b), with a mean coverage value of 0.84 ± 0.02. (c) Spatial Raman mapping of the frequency $\omega_{G2}$ band deduced from a fitting procedure, two examples of which are reported for selected Raman spectra in panel (d). The two exemplary spectra correspond to two points (circle and star) of panel (a).

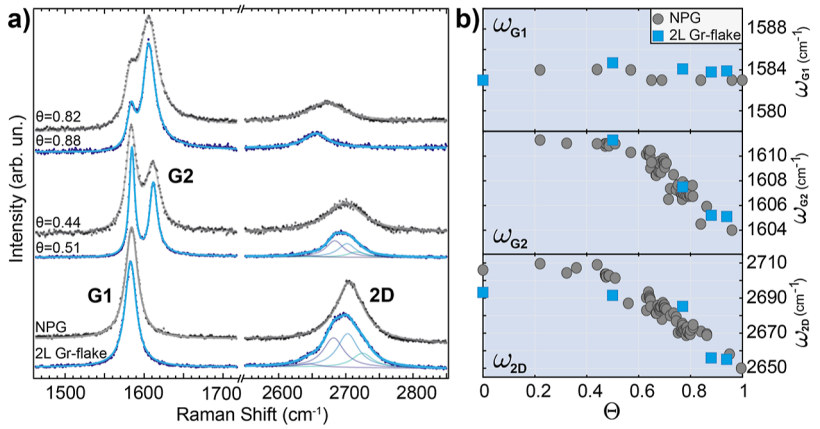


**Figure 5.** (a) Comparison of NPG (dark grey line) and 2L Gr (dark blue line) Raman spectra as a function of K coverage $\left(\Theta = \frac{I_{G2}}{I_{G1}+I_{G2}}\right)$. (b) Frequency ($\omega$) evolution of the G1, G2, and 2D Raman bands as a function of K coverage, for both K-NPG (dark gray dots) and K/2L Gr (dark blue squares).

the Gaussian-like histogram of the Θ values (panel b) with a mean value of $\mu$ = 0.84 and standard deviation $\sigma$ = 0.02.

Each pixel of the spatial distribution contains a Raman spectrum, that has been fitted using two Lorentzian curves to reproduce the G1 and G2 bands. An example of such a fitting procedure is reported in panel (d), where two different spectra are displayed, respectively, from a lower (circle) and a higher (star) doping region. The G2 band energy spatial distribution ($\omega_{G2}$), reported in panel (c), unveils higher doping regions with softer G2 peaks and lower doping regions with stiffer G2 bands. The homogeneity observed in the micro-Raman mapping ensures an averaged charging effect over all the NPG sample.

In order to have a deeper understanding of the different contributions and a further confirmation of the charge transfer effects on the vibrational response of K-doped Gr, we have performed an analogous K doping on the flat 2L Gr flake. In Figure 5a, a selected set of Raman spectra of K-doped NPG compared with a K-doped 2L Gr flake is shown. We observe that the spectral evolution on 2L Gr (blue curves) is rather similar to that on NPG (dark gray curves), with the formation of the G2 band fingerprint of the charge migration, and a gradual reduction of the 2D mode, in qualitative agreement with previous Raman data on K-doped graphite compounds and few-layer Gr systems.[30,31,33]



https://doi.org/10.1021/acsomega.4c03543
ACS Omega 2024, 9, 39546−39553

As far as the 2D band is concerned, the progressive intensity reduction upon K doping can be attributed to an increased electron−electron (e−e) scattering rate ($\gamma_{ee}$) with increasing charge carrier density. In fact, theoretical predictions[37] evaluate a linear dependence of $\gamma_{ee}$ with the Fermi level shift $\Delta E$, while the intensity of the 2D mode scales as $\gamma_{ee}^{-2}$. Furthermore, the 2D band line shape for the 2L Gr flake[24] becomes narrower and more symmetric upon doping. This effect suggests an intercalation of K adatoms increasing the interlayer spacing of the 2L Gr flake, therefore weakening the interactions between the layers, resulting in a single Raman scattering process for the 2D mode. The 2D band line shape is symmetric in the NPG sample because of the turbostratic arrangement of its weakly interacting layers, and the eventual K intercalated atoms are not expected to affect the 2D band line shape.

The coverage dependence of the frequency of the main Raman bands (Figure 5b) is determined by a fitting with Lorentzian components for the pristine and K-doped spectra for a broad set of measurements, some of which are reported in panel (a).

A clear softening of the frequency for the G2 and 2D modes is present for both the NPG and the 2L Gr flake. In particular, for $\Theta > 0.5$, the G2 frequency varies from 1611 to 1604 $cm^{-1}$, while the 2D band frequency varies from 2705 to 2650 $cm^{-1}$ for the NPG, and from 2692 to 2655 $cm^{-1}$ for the 2L Gr flake. This is a further confirmation of the similarity between 2L Gr and NPG, and we can propose a common interpretation of the observed frequency shifts.

The frequency shift $\Delta\omega_G$ of the G band between the undoped and the fully doped case can be due to several reasons. First of all, the electron doping, moving the Fermi level up to a position of higher $\pi^*$ state density, changes the $\pi$ electron optical spectrum, and thus modifies the EPC. The breakdown of the BO approximation drives the renormalization of the phonon frequencies, inducing a stiffening of the G mode (leading to the observed G2 band), as reported in several experimental papers.[1−4,6] Another cause of the frequency shift is the tensile strain associated with the charge donation, as observed for gate voltage-doped Gr.[2,36] However, the presence of the adsorbed and/or intercalated potassium adatoms in Gr can induce a steric strain effect. A quantitative explanation of the observed $\omega_{G2}$ frequency shift must include both the phonon renormalization due to the breakdown of the BO approximation and the lattice expansion. This model, introduced by Lazzeri and Mauri,[2] considers the effect of the increased charge doping by summing three contributions

$$\Delta\omega_G = \alpha' E_F + \frac{\alpha'\hbar\omega_0}{4}\log\left|\frac{E_F - \hbar\omega_0/2}{E_F + \hbar\omega_0/2}\right| + \Delta\omega_{strain}(E_F) \quad (1)$$

The first two addenda (*dynamic terms*) provide a positive shift of the G component, and they are related to the EPC, while the third one (*static term*) determines a negative shift of the G peak and is related to charge-induced lattice expansion. In eq 1, $\alpha'$ is associated with the EPC by $\lambda = 2\pi\alpha'$, while $\hbar\omega_0$ is the unperturbed G band Raman frequency. In a rigid band model, where the Gr bands are preserved upon doping and the Gr lattice is unperturbed, the tensile strain induced by the increased charge density has been calculated via static perturbation theory on the DFT total energy.[2] The Fermi level shift ($E_F$ = 0.6 eV) measured at the maximum K doping ($\Theta$ = 1), corresponds to an estimated tensile strain of $\varepsilon \sim$ 0.05%, which implies a shift $\Delta\omega_{G2} = -2.85$ $cm^{-1}$ (see Supporting Information), where the injected charge softens the bonds leading to a tensile strain in the system. However, at maximum doping we observe a shift $\Delta\omega_{G2} = -7$ $cm^{-1}$, larger than the one expected from charge-induced strain calculation. Thus, an additional strain mechanism related to a steric effect due to the presence of the AM in the Gr mesh should be considered.

The additional steric strain, including the $\Delta\omega_{G2}$ missing contribution (−4.15 $cm^{-1}$), results in $\varepsilon$ = 0.08% (see Supporting Information). The latter sums up to the charge-induced strain ($\varepsilon$ = 0.05%) giving a total strain of $\varepsilon$ = 0.13% in the present K-doped Gr system.

We were able to distinguish so far the charge and steric strain from the dynamic contribution to the Raman $\Delta\omega_{G2}$ frequency shift, thus a direct information on the electron−phonon interaction $\alpha'$ can be easily deduced. At K-doping saturation, the dynamic term is $\Delta\omega_G = 20$ $cm^{-1}$ and the static $\Delta\omega_{strain} = -7$ $cm^{-1}$. By inverting eq 1, we obtain $\alpha' = (5.58 \pm 0.5) \times 10^{-3}$, i.e., $\lambda = (3.5 \pm 0.4) \times 10^{-2}$, which is ∼30% larger than typical values on gate-doped Gr[1,3,12] and on most of liquid-gated Gr.[36] This larger strength of the electron−phonon interaction accounts for the additional effective presence of the AM in the Gr mesh. Even larger EPC (by ∼90%) has been derived by ARPES in heavily Cs-doped supported Gr,[16] although we remind that photoemission data can overestimate the EPC.[14]

## CONCLUSIONS

A fine control of the electronic/vibrational response in chemically doped free-standing Gr, without a detrimental effect of the substrate and free of contaminants, unveils a notable EPC. The original combined UHV micro-Raman and XPS setup allows a comparison of NPG and the 2-layer Gr flake, at increasing potassium doping deposited in situ. From the analysis of the vibrational response, correlated with the charge associated with the plasmon in the upper Dirac cone and the Fermi level shift, we estimate an electron−phonon interaction parameter $\lambda$ of K-doped Gr larger than that deduced in electronic doping by gate voltages. Furthermore, we identify a contribution to the Raman frequency shift due a tensile strain related to a steric lattice expansion associated with the presence of the K adatoms, similar to that in turbostratic NPG and bilayer Gr.

## EXPERIMENTAL METHODS

**Sample Preparation.** NPG was grown through a nanoporous Ni template by means of chemical vapor deposition (CVD). Ingots of $Ni_{30}Mn_{70}$ alloy were first synthesized by melting pure Ni and Mn in an Ar-protected arc melting furnace, then they were annealed to become microstructured and composition-homogeneous alloys, then rolled into thin films. In order to obtain the nanoporous Ni template, the NiMn alloy sheet was chemically dealloyed with 0.5 M ammonium sulfate for nanoporous Ni. Nanoporous Ni was used as the CVD substrate, and benzene was then used as a precursor for CVD Gr growth at 900 °C for 5 min. The Gr sheet covering nanoporous Ni and presenting its same three-dimensional morphology was subsequently exfoliated by chemical dissolution of the Ni template by 1.0 M hydrochloric acid. The synthesis and preparation process are described in detail elsewhere.[19−21,38−41] Prior to the spectroscopic data


https://doi.org/10.1021/acsomega.4c03543
ACS Omega 2024, 9, 39546−39553

acquisition in each UHV apparatus in each laboratory, the NPG samples were degassed at 600−620 °C for several hours to remove contaminants from air exposure.[42]

The few-layer Gr flake has been mechanically exfoliated directly from pure natural graphite and sequentially transferred by an all-dry deterministic transfer procedure[43,44] on a $SiO_2$/Si substrate, by using a polydimethylsiloxane stamp (Gel-Film WF × 46.0 mil by Gel-Pak). Details of the flake preparation and transfer are available in the Supporting Information.

Potassium was sublimated in UHV (in the $10^{-10}$ mbar range) by using commercial SAES getter dispensers, after overnight degassing at currents slightly below the sublimation onset. The sublimation rate was kept as constant as possible in each measurement set, and it was similar in the different UHV chambers, by using equivalent dispensers mounted in each apparatus.

**Photoelectron and Raman Spectroscopy.** The integrated high-resolution XPS and micro-Raman spectroscopy experiments were performed at the SmartLab departmental laboratory[45] (see Supporting Information) of the Department of Physics at Sapienza University of Rome. This newly conceived apparatus combines a novel setup of electron- and optical-microspectroscopies, all in UHV with base pressure in the range of high $10^{-11}$ mbar in all the stages. The system is also equipped with a UHV-interconnected preparation chamber with all ancillary facilities for sample cleaning and AM deposition. XPS measurements were carried out using an Al K$\alpha$ monochromatic (1486.6 eV) source (SPECS XR50 MF), and the electrons were analyzed by a hemispherical SPECS PHOIBOS 150 analyzer from the SPECS group with an energy resolution of about 0.4 eV. The Raman spectroscopy experiments were carried out in the novel UHV setup using as an excitation source, a single frequency ND/YV04 laser, at 532.2 nm wavelength. The power of the laser was kept below 250 $\mu$W on the sample to avoid any kind of sample damage. The system is equipped with a 50 cm focal-length monochromator with a 300 and 1200 grooves/mm grating, and the signal is detected by a back-illuminated liquid N2-cooled Si CCD camera. The Raman sample holder is mounted on a hexapod piezoelectric stage, which can be moved with steps of 50 nm, while the spatial resolution of approximately 500 nm is limited by the laser source wavelength and focal spot.

**EELS.** EELS measurements were performed at the LSAM-STAR laboratory of the Università della Calabria, in the reflection geometry at $E_p$ = 105.5 eV, using the electron source SPECS EQ 22/35 and the hemispherical electron energy analyzer SPECS PHOIBOS 150. The angle between the analyzer and an electron gun was about 35°. The full-width at the half-maximum of the reflection peak for $E_p$ = 105.5 eV was about 0.5 eV. The base pressure during all measurements was less than $1 \times 10^{-9}$ mbar.

## ■ ASSOCIATED CONTENT

### Supporting Information

The Supporting Information is available free of charge at https://pubs.acs.org/doi/10.1021/acsomega.4c03543.

Description and a photograph of the new advanced setup for combined UHV Raman and XPS measurements, details on the Gr flake preparation and transfer procedure, transmittance optical image of the Gr flake sample, and details on the strain calculation (PDF)

## ■ AUTHOR INFORMATION


### Corresponding Authors

**Dario Marchiani** − *Physics Department, Sapienza University of Rome, 00185 Rome, Italy*; Email: dario.marchiani@uniroma1.it

**Maria Grazia Betti** − *Physics Department, Sapienza University of Rome, 00185 Rome, Italy*; orcid.org/0000-0002-6244-0306; Email: mariagrazia.betti@uniroma1.it

### Authors

**Riccardo Frisenda** − *Physics Department, Sapienza University of Rome, 00185 Rome, Italy*

**Carlo Mariani** − *Physics Department, Sapienza University of Rome, 00185 Rome, Italy*; orcid.org/0000-0002-7979-1700

**Marco Sbroscia** − *Physics Department, Sapienza University of Rome, 00185 Rome, Italy*

**Tommaso Caruso** − *Dipartimento di Fisica, Università della Calabria, 87036 Arcavacata di Rende, Cosenza, Italy; Laboratorio di Spettroscopia Avanzata dei Materiali, STAR IR, Università della Calabria, 87036 Rende, Cosenza, Italy*

**Oreste De Luca** − *Dipartimento di Fisica, Università della Calabria, 87036 Arcavacata di Rende, Cosenza, Italy; Laboratorio di Spettroscopia Avanzata dei Materiali, STAR IR, Università della Calabria, 87036 Rende, Cosenza, Italy*

**Marco Papagno** − *Dipartimento di Fisica, Università della Calabria, 87036 Arcavacata di Rende, Cosenza, Italy; Laboratorio di Spettroscopia Avanzata dei Materiali, STAR IR, Università della Calabria, 87036 Rende, Cosenza, Italy*

**Daniela Pacilé** − *Dipartimento di Fisica, Università della Calabria, 87036 Arcavacata di Rende, Cosenza, Italy*; orcid.org/0000-0001-6219-3889

**Samuel Jeong** − *Institute of Applied Physics, Graduate School of Pure and Applied Sciences, University of Tsukuba, 305-8573 Tsukuba, Japan*; orcid.org/0000-0003-2231-7271

**Yoshikazu Ito** − *Institute of Applied Physics, Graduate School of Pure and Applied Sciences, University of Tsukuba, 305-8573 Tsukuba, Japan*; orcid.org/0000-0001-8059-8396

Complete contact information is available at: https://pubs.acs.org/10.1021/acsomega.4c03543


### Notes

The authors declare no competing financial interest.

## ■ ACKNOWLEDGMENTS

This work was partially supported by the PRIN Grants TUNES (2022NXLTYN, 2D-FRONTIERS (20228879FT) and by by "Progetto STAR2-PIR01_00008" of the Italian Ministero dell'Università e della Ricerca (MUR), by European Union-Next Generation EU under PNRR-NEST project ENERGY SUSTAINABLE TRANSITION-NETWORK 4 Spoke 6 Next Generation EU-PE0000021, by Sapienza Ateneo and Avvio alla ricerca funds, by JSPS-Kakenhi (grant numbers JP21H02037 and JP23K17661), and by CASIO Science Promotion Foundation.

## ■ REFERENCES

(1) Pisana, S.; Lazzeri, M.; Casiraghi, C.; Novoselov, K. S.; Geim, A. K.; Ferrari, A. C.; Mauri, F. Breakdown of the adiabatic Born−Oppenheimer approximation in graphene. *Nat. Mater.* **2007**, *6*, 198−201.

(2) Lazzeri, M.; Mauri, F. Nonadiabatic Kohn Anomaly in a Doped Graphene Monolayer. *Phys. Rev. Lett.* **2006**, *97*, 266407.

(3) Yan, J.; Zhang, Y.; Kim, P.; Pinczuk, A. Electric Field Effect Tuning of Electron-Phonon Coupling in Graphene. *Phys. Rev. Lett.* **2007**, *98*, 166802.
(4) Das, A.; Pisana, S.; Chakraborty, B.; Piscanec, S.; Saha, S. K.; Waghmare, U. V.; Novoselov, K. S.; Krishnamurthy, H. R.; Geim, A. K.; Ferrari, A. C.; Sood, A. K. Monitoring dopants by Raman scattering in an electrochemically top-gated graphene transistor. *Nat. Nanotechnol.* **2008**, *3*, 210−215.
(5) Das, A.; Chakraborty, B.; Piscanec, S.; Pisana, S.; Sood, A. K.; Ferrari, A. C. Phonon renormalization in doped bilayer graphene. *Phys. Rev. B: Condens. Matter Mater. Phys.* **2009**, *79*, 155417.
(6) Howard, C. A.; Dean, M. P. M.; Withers, F. Phonons in potassium-doped graphene: The effects of electron-phonon interactions, dimensionality, and adatom ordering. *Phys. Rev. B: Condens. Matter Mater. Phys.* **2011**, *84*, 241404R.
(7) Grüneis, A.; Attaccalite, C.; Rubio, A.; Vyalikh, D. V.; Molodtsov, S. L.; Fink, J.; Follath, R.; Eberhardt, W.; Büchner, B.; Pichler, T. Electronic structure and electron-phonon coupling of doped graphene layers in $KC_8$. *Phys. Rev. B: Condens. Matter Mater. Phys.* **2009**, *79*, 205106.
(8) Siegel, D. A.; Park, C.-H.; Hwang, C.; Deslippe, J.; Fedorov, A. V.; Louie, S. G.; Lanzara, A. Many-body interactions in quasi-freestanding graphene. *Proc. Natl. Acad. Sci. U.S.A.* **2011**, *108*, 11365−11369.
(9) Bianchi, M.; Rienks, E. D. L.; Lizzit, S.; Baraldi, A.; Balog, R.; Hornekær, L.; Hofmann, P. Electron-phonon coupling in potassium-doped graphene: Angle-resolved photoemission spectroscopy. *Phys. Rev. B: Condens. Matter Mater. Phys.* **2010**, *81*, 041403.
(10) Ludbrook, B. M.; Levy, G.; Nigge, P.; Zonno, M.; Schneider, M.; Dvorak, D. J.; Veenstra, C. N.; Zhdanovich, S.; Wong, D.; Dosanjh, P.; et al. Evidence for superconductivity in Li-decorated monolayer graphene. *Proc. Natl. Acad. Sci. U.S.A.* **2015**, *112*, 11795−11799.
(11) Metten, D.; Froehlicher, G.; Berciaud, S. Monitoring electrostatically-induced deflection, strain and doping in suspended graphene using Raman spectroscopy. *2D Mater.* **2016**, *4*, 014004.
(12) Sonntag, J.; Watanabe, K.; Taniguchi, T.; Beschoten, B.; Stampfer, C. Charge carrier density dependent Raman spectra of graphene encapsulated in hexagonal boron nitride. *Phys. Rev. B* **2023**, *107*, 075420.
(13) Childres, I.; Jauregui, L. A.; Chen, Y. P. Raman spectra and electron-phonon coupling in disordered graphene with gate-tunable doping. *J. Appl. Phys.* **2014**, *116*, 233101.
(14) Calandra, M.; Mauri, F. Electron-phonon coupling and electron self-energy in electron-doped graphene: Calculation of angular-resolved photoemission spectra. *Phys. Rev. B: Condens. Matter Mater. Phys.* **2007**, *76*, 205411.
(15) Parret, R.; Paillet, M.; Huntzinger, J.-R.; Nakabayashi, D.; Michel, T.; Tiberj, A.; Sauvajol, J.-L.; Zahab, A. A. In Situ Raman Probing of Graphene over a Broad Doping Range upon Rubidium Vapor Exposure. *ACS Nano* **2013**, *7*, 165−173.
(16) Hell, M. G.; Ehlen, N.; Senkovskiy, B. V.; Hasdeo, E. H.; Fedorov, A.; Dombrowski, D.; Busse, C.; Michely, T.; di Santo, G.; Petaccia, L.; Saito, R.; Grüneis, A. Resonance Raman Spectrum of Doped Epitaxial Graphene at the Lifshitz Transition. *Nano Lett.* **2018**, *18*, 6045−6056.
(17) Di Bernardo, I.; Avvisati, G.; Chen, C.; Avila, J.; Asensio, M. C.; Hu, K.; Ito, Y.; Hines, P.; Lipton-Duffin, J.; Rintoul, L.; Motta, N.; Mariani, C.; Betti, M. G. Topology and doping effects in three-dimensional nanoporous graphene. *Carbon* **2018**, *131*, 258−265.
(18) Di Bernardo, I.; Avvisati, G.; Mariani, C.; Motta, N.; Chen, C.; Avila, J.; Asensio, M. C.; Lupi, S.; Ito, Y.; Chen, M.; Fujita, T.; Betti, M. G. Two-Dimensional Hallmark of Highly Interconnected Three-Dimensional Nanoporous Graphene. *ACS Omega* **2017**, *2*, 3691−3697.
(19) Ito, Y.; Qiu, H.-J.; Fujita, T.; Tanabe, Y.; Tanigaki, K.; Chen, M. Bicontinuous Nanoporous N-doped Graphene for the Oxygen Reduction Reaction. *Adv. Mater.* **2014**, *26*, 4145−4150.
(20) Ito, Y.; Tanabe, Y.; Qiu, H.-J.; Sugawara, K.; Heguri, S.; Tu, N. H.; Huynh, K. K.; Fujita, T.; Takahashi, T.; Tanigaki, K.; et al. High-Quality Three-Dimensional Nanoporous Graphene. *Angew. Chem., Int. Ed.* **2014**, *53*, 4822−4826.
(21) Ito, Y.; Cong, W.; Fujita, T.; Tang, Z.; Chen, M. High Catalytic Activity of Nitrogen and Sulfur Co-Doped Nanoporous Graphene in the Hydrogen Evolution Reaction. *Angew. Chem., Int. Ed.* **2015**, *54*, 2131−2136.
(22) Nair, R. R.; Blake, P.; Grigorenko, A. N.; Novoselov, K. S.; Booth, T. J.; Stauber, T.; Peres, N. M. R.; Geim, A. K. Fine Structure Constant Defines Visual Transparency of Graphene. *Science* **2008**, *320*, 1308.
(23) Ferrari, A. C.; Meyer, J. C.; Scardaci, V.; Casiraghi, C.; Lazzeri, M.; Mauri, F.; Piscanec, S.; Jiang, D.; Novoselov, K. S.; Roth, S.; et al. Raman Spectrum of Graphene and Graphene Layers. *Phys. Rev. Lett.* **2006**, *97*, 187401.
(24) Malard, L.; Pimenta, M.; Dresselhaus, G.; Dresselhaus, M. Raman spectroscopy in graphene. *Phys. Rep.* **2009**, *473*, 51−87.
(25) Marchiani, D.; Tonelli, A.; Mariani, C.; Frisenda, R.; Avila, J.; Dudin, P.; Jeong, S.; Ito, Y.; Magnani, F. S.; Biagi, R.; De Renzi, V.; Betti, M. G. Tuning the Electronic Response of Metallic Graphene by Potassium Doping. *Nano Lett.* **2023**, *23*, 170−176.
(26) Lu, J.; Loh, K. P.; Huang, H.; Chen, W.; Wee, A. T. S. Plasmon dispersion on epitaxial graphene studied using high-resolution electron energy-loss spectroscopy. *Phys. Rev. B: Condens. Matter Mater. Phys.* **2009**, *80*, 113410.
(27) Pisarra, M.; Sindona, A.; Gravina, M.; Silkin, V. M.; Pitarke, J. M. Dielectric screening and plasmon resonances in bilayer graphene. *Phys. Rev. B* **2016**, *93*, 035440.
(28) Politano, A.; Marino, A. R.; Formoso, V.; Farías, D.; Miranda, R.; Chiarello, G. Quadratic Dispersion and Damping Processes of $\pi$ Plasmon in Monolayer Graphene on Pt(111). *Plasmonics* **2012**, *7*, 369−376.
(29) Liou, S. C.; Shie, C.-S.; Chen, C. H.; Breitwieser, R.; Pai, W. W.; Guo, G. Y.; Chu, M.-W. $\pi$-plasmon dispersion in free-standing graphene by momentum-resolved electron energy-loss spectroscopy. *Phys. Rev. B: Condens. Matter Mater. Phys.* **2015**, *91*, 045418.
(30) Chacón-Torres, J. C.; Wirtz, L.; Pichler, T. Manifestation of Charged and Strained Graphene Layers in the Raman Response of Graphite Intercalation Compounds. *ACS Nano* **2013**, *7*, 9249−9259.
(31) Chacón-Torres, J. C.; Wirtz, L.; Pichler, T. Raman spectroscopy of graphite intercalation compounds: Charge transfer, strain, and electron−phonon coupling in graphene layers. *Phys. Status Solidi B* **2014**, *251*, 2337−2355.
(32) Wang, Y.; Puech, P.; Gerber, I.; Pénicaud, A. Resonant Raman scattering of graphite intercalation compounds KC8, KC24, and KC36. *J. Raman Spectrosc.* **2014**, *45*, 219−223.
(33) Szirmai, P.; Márkus, B. G.; Chacón-Torres, J. C.; Eckerlein, P.; Edelthalhammer, K.; Englert, J. M.; Mundloch, U.; Hirsch, A.; Hauke, F.; Náfrádi, B.; Forró, L.; Kramberger, C.; Pichler, T.; Simon, F. Characterizing the maximum number of layers in chemically exfoliated graphene. *Sci. Rep.* **2019**, *9*, 19480.
(34) Nemanich, R. J.; Solin, S. A.; Güerard, D. Raman scattering from intercalated donor compounds of graphite. *Phys. Rev. B: Solid State* **1977**, *16*, 2965−2972.
(35) Solin, S. A.; Caswell, N. Raman scattering from alkali graphite intercalation compounds. *J. Raman Spectrosc.* **1981**, *10*, 129−135.
(36) Froehlicher, G.; Berciaud, S. Raman spectroscopy of electrochemically gated graphene transistors: Geometrical capacitance, electron-phonon, electron-electron, and electron-defect scattering. *Phys. Rev. B: Condens. Matter Mater. Phys.* **2015**, *91*, 205413.
(37) Basko, D. M.; Piscanec, S.; Ferrari, A. C. Electron-electron interactions and doping dependence of the two-phonon Raman intensity in graphene. *Phys. Rev. B: Condens. Matter Mater. Phys.* **2009**, *80*, 165413.
(38) Ito, Y.; Tanabe, Y.; Han, J.; Fujita, T.; Tanigaki, K.; Chen, M. Multifunctional Porous Graphene for High-Efficiency Steam Generation by Heat Localization. *Adv. Mater.* **2015**, *27*, 4302−4307.


https://doi.org/10.1021/acsomega.4c03543
*ACS Omega* 2024, 9, 39546−39553

(39) Hu, K.; Qin, L.; Zhang, S.; Zheng, J.; Sun, J.; Ito, Y.; Wu, Y. Building a Reactive Armor Using S-Doped Graphene for Protecting Potassium Metal Anodes from Oxygen Crossover in K−O2 Batteries. *ACS Energy Lett.* **2020**, *5*, 1788−1793.
(40) Tanabe, Y.; Ito, Y.; Sugawara, K.; Koshino, M.; Kimura, S.; Naito, T.; Johnson, I.; Takahashi, T.; Chen, M. Dirac Fermion Kinetics in 3D Curved Graphene. *Adv. Mater.* **2020**, *32*, 2005838.
(41) Tanabe, Y.; Ito, Y.; Sugawara, K.; Jeong, S.; Ohto, T.; Nishiuchi, T.; Kawada, N.; Kimura, S.; Aleman, C. F.; Takahashi, T.; Kotani, M.; Chen, M. Coexistence of Urbach-Tail-Like Localized States and Metallic Conduction Channels in Nitrogen-Doped 3D Curved Graphene. *Adv. Mater.* **2022**, *34*, 2205986.
(42) Abdelnabi, M. M. S.; Izzo, C.; Blundo, E.; Betti, M. G.; Sbroscia, M.; Di Bella, G.; Cavoto, G.; Polimeni, A.; García-Cortés, I.; Rucandio, I.; Moroño, A.; Hu, K.; Ito, Y.; Mariani, C. Deuterium Adsorption on Free-Standing Graphene. *Nanomaterials* **2021**, *11*, 130.
(43) Zhao, Q.; Wang, T.; Ryu, Y. K.; Frisenda, R.; Castellanos-Gomez, A. An inexpensive system for the deterministic transfer of 2D materials. *J. Phys. Mater.* **2020**, *3*, 016001.
(44) Castellanos-Gomez, A.; Buscema, M.; Molenaar, R.; Singh, V.; Janssen, L.; van der Zant, H. S. J.; Steele, G. A. Deterministic transfer of two-dimensional materials by all-dry viscoelastic stamping. *2D Mater.* **2014**, *1*, 011002.
(45) SmartLab. https://sites.google.com/uniroma1.it/smartlab, November, 2023 (accessed 8th May 2024).



https://doi.org/10.1021/acsomega.4c03543
*ACS Omega* 2024, 9, 39546−39553